RESEARCH ARTICLE

ADVANCED OPTICAL MATERIALS
www.advopticalmat.de

Observation of Laser Cooling on an Electric-Dipole-Allowed Transition in Cr^{3+}:LiSAF Crystal

Junior Reis Silva, Luis Humberto da Cunha Andrade, Sandro Marcio Lima, Antônio Carlos Bento, Tomaz Catunda, and Stephen Colby Rand*

In this work, an electric dipole allowed transition in two Cr^{3+}:LiSAF samples is investigated for the purpose of optical refrigeration. A cooling efficiency approaching 10% is experimentally determined using a mode-mismatched dual-beam thermal lens method with excitation wavelength, λ_{exc}, of 1 µm in an unoriented 1% Cr^{3+}:LiSAF, which has an average emission wavelength, $\langle\lambda_{em}\rangle$, of 850 nm. In an oriented 4% Cr^{3+}:LiSAF sample, the efficiency reached (but does not exceed) the threshold for cooling when excited with π-polarized light. These results suggest that Cr^{3+}:LiSAF can approach an ideal cooling efficiency $\sim (\lambda_{exc} - \langle\lambda_{em}\rangle)/\langle\lambda_{em}\rangle \sim$ 20% with excitation ≈1µm. Additionally, this analysis indicates that parasitic background absorption rather than upconversion or excited state absorption limits the cooling at higher Cr^{3+} concentrations.

1. Introduction

To date, laser-induced fluorescent cooling of solids has been most successful in Yb^{3+} -doped materials. After the first observation of cooling in a Yb^{3+}:ZBLAN glass,[1] several materials were investigated, and the Yb^{3+}:YLF fluoride crystal became the first solid-state to cool below 100 Kelvin.[2] Other trivalent rare earths have demonstrated the cooling effect,[3–5] but not with the same efficiency or minimum temperature as Yb^{3+}:YLF crystals with low background impurity levels. Other ions and host materials nevertheless continue to be investigated because of interest in faster, more efficient cooling and the need to achieve refrigeration in specific solid-state platforms with important technological applications. For example, the experimental report of optical refrigeration in Yb^{3+}-doped silica glass has attracted attention recently because of its implications for self-cooled and fiber-based photonics.[6] However, the low transition rate of Yb^{3+}-doped compounds generally hinders the prospects for optical cooling applications in advanced photonic technology because it results in small optical absorption coefficients, slow cooling, and low efficiency. Moreover, cumbersome optical enhancement cavities are often needed to raise the efficiency of optical refrigeration to levels comparable with more established cooling methods.

Allowed electric-dipole (ED) transitions have been investigated for use in the laser cooling of solids[7] due to the high transition rate they incur when compared with the forbidden transitions of Yb^{3+}. This characteristic, together with the large Stokes shifts between absorption and emission spectra commonly observed in this kind of transition, holds the prospect of improving cooling efficiency. Many ions have been explored to achieve cooling with ED-allowed transitions in solids, but to date no experiment has succeeded in attaining net cooling.[7] The challenges of using allowed transitions for cooling are mostly related to energy-transfer upconversion (ETU), also known as Auger upconversion, and excited-state absorption (ESA) transitions that result in the deposition of extra heat into the system. Not surprisingly, these sources of internal heating also lower the cooling efficiency on forbidden transitions in rare earth ions like Er^{3+}, Tm^{3+}, and Ho^{3+}, which can undergo ETU or ESA, and generally exhibit lower efficiencies than Yb^{3+}-doped materials.

Several Cr^{3+}-doped crystals were previously investigated for the purpose of optical refrigeration, but no cooling was observed.[8,9] However, the crystals selected in early experiments were mostly oxides with high or intermediate crystal fields, as defined by Tanabe-Sugano (Dq/B > 2.3). In these materials, the ^2E state of Cr^{3+} is a metastable state.[10] From this level, excited ions

J. R. Silva, L. H. da C. Andrade, S. M. Lima
Programa de Pós-Graduação em Recursos Naturais
Universidade Estadual de Mato Grosso do Sul
Dourados, MS 79804-970, Brazil
E-mail: juniorrsilva@uems.br
A. C. Bento
Departamento de Física
Universidade Estadual de Maringá
Maringá, PR 87020-900, Brazil
T. Catunda
Instituto de Física de São Carlos
Universidade de São Paulo
IFSC-USP
São Carlos, SP 13566–590, Brazil
S. C. Rand
Division of Applied Physics
University of Michigan
Ann Arbor, MI 48109, USA

The ORCID identification number(s) for the author(s) of this article can be found under https://doi.org/10.1002/adom.202403222

DOI: 10.1002/adom.202403222

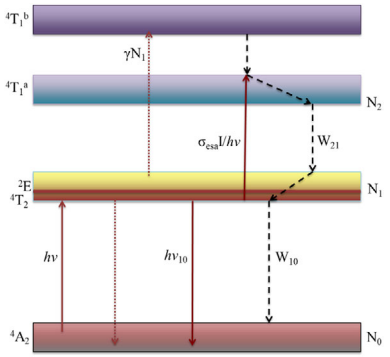

Figure 1. Simplified energy level diagram for the Cr^{3+}:LiSAF system.

decay to the ground state by a forbidden ED transition, which limits the theoretical cooling efficiency to a very low value, as discussed in the review by Hehlen.[7] On the other hand, in low crystal field materials (Dq/B < 2.3) the $^4T_2$ level descends in energy to become the lowest-lying excited state. Because the $^4T_2$ – $^4A_2$ transition is spin-allowed, and the low crystal field at the Al^{3+} substitutional site in fluorides like Cr^{3+}:LiSAF contains an odd-parity component[11] it results in an ED-allowed emission (as well as absorption) between the first excited state and the ground state. This could enable fast cooling with improved efficiency. Moreover, crystalline Cr^{3+}:LiSAF is a laser material with an external quantum efficiency near unity that might support not only fast laser cooling but also operation as a tunable, radiation-balanced laser.[12] It has a broad absorption band, does not suffer from concentration quenching of fluorescence, and can be grown with high optical quality and minimal background absorption.[10] Therefore, in this work, we investigated Cr^{3+}:LiSAF with these potential applications in mind, and for the first time report laser cooling using an ED-allowed transition in a Cr^{3+}-doped material.

1.1. Theory

In its simplest form, laser-induced cooling of solid-state materials is accomplished by absorption from the ground to an excited state and subsequent anti-Stokes fluorescence. As a result, standard cooling theory considers only radiative and non-radiative decay processes from the metastable excited state. In Cr^{3+}-doped materials however, excitation is generally followed by additional processes, such as ESA and ETU. In Cr^{3+}:LiSAF crystals, these processes occur along with the ordinary radiative and non-radiative relaxations from the $^4T_2$ excited state to the $^4A_2$ ground state,[10,13] so that a more extended analysis is required. That is, for this class of materials, cooling theory should include these processes to interpret experimental results properly.

In **Figure 1**, the processes and transitions involved in optical excitation of the Cr^{3+}:LiSAF system are illustrated. The solid upward arrow on the $^4A_2 \rightarrow {}^4T_2$ transition represents the initial absorptive step, while the solid downward arrow indicates the radiative decay from the $^4T_2$ level to the ground state. The pair of dotted arrows depict an Auger ETU process originating from population in the excited state, and ESA is represented by a solid upward arrow on the $^4T_2 \rightarrow {}^4T_1{}^a$ transition. The dashed lines represent non-radiative decay pathways. To analyze the cooling efficiency for the system of Figure 1, we begin by writing down rate equations for the number of dopant ions in the first two excited states and solving them in the steady state limit, as follows:

$$\frac{dN_1}{dt} = \left[\sigma_{gsa}N_0 - \sigma_{esa}N_1\right]\frac{I}{h\upsilon} - \frac{N_1}{\tau} - \gamma\left(N_1\right)^2 + W_{21}N_2 \tag{1}$$

$$\frac{dN_2}{dt} = \sigma_{esa}\,N_1\frac{I}{h\upsilon} - W_{21}N_2 \tag{2}$$

Equation (1) describes the population dynamics of the first excited state. The first and second terms represent the ground and excited state absorptions, where σ_{gsa} and σ_{esa} are the ground and excited state absorption cross-sections, respectively. N_i is the population density of the ith state. The areal density of excitation photons per second is given by $I/h\upsilon$, where I is the intensity and $h\upsilon$ the photon energy of incident radiation. The third term includes the radiative and non-radiative decays from the $^4T_2$ excited state, by introducing the fluorescence lifetime $\tau = (W_{rad} + W_{10})^{-1}$. The fourth term accounts for ETU, γ being the upconversion rate parameter,[14,15] and the last term describes non-radiative decay from the second to the first excited state at a rate of W_{21}.

The rate per unit volume at which heat energy (H) is generated in this system can be written as:

$$H = \sigma_{gsa}\,N_0\frac{I}{h\upsilon}\left(h\upsilon - h\upsilon_{10}\right) + \sigma_{esa}N_1\frac{I}{h\upsilon}\left(h\upsilon - h\upsilon_{21}\right) + W_{21}N_2h\upsilon_{21} + W_{10}N_1h\upsilon_{10} + \gamma\left(N_1\right)^2h\upsilon_{10} + \alpha_bI \tag{3}$$

where $h\upsilon_{ij}$ and W_{ij} represent the energies and non-radiative relaxation rates between the i and j states and α_b is the parasitic background absorption coefficient associated with undesirable impurities in the sample. The fraction of absorbed energy converted into heat is then given by:

$$\varphi = \frac{H}{\left(\sigma_{gsa}N_0 + \sigma_{esa}N_1 + \alpha_b\right)I} \tag{4}$$

By substituting Equation (3) into Equation (4) and solving for N_0 and N_1 in the steady-state, one can calculate the cooling efficiency (η_c) by simply negating φ. In this way we find,

$$\eta_c = -\varphi = \frac{\eta_{ext}\eta_{abs}}{1 + \eta_{abs}\left(\delta + \xi\right)}\frac{\lambda_{exc}}{\langle\lambda_{em}\rangle} - 1 \tag{5}$$

where $\eta_{ext} = 1 - W_{10}\tau$, $\eta_{abs} = \alpha/(\alpha + \alpha_b)$, α is the absorption coefficient of the coolant ions and α_b is the parasitic background absorption coefficient at the excitation wavelength. In Equation (5) the ESA process contributes via the factor,

$$\xi = \sigma_{esa}\,\tau\,\frac{I}{h\nu} = \frac{\sigma_{esa}}{\sigma_{gsa}}\frac{I}{I_{sat}} \tag{6}$$

where $I_{sat} \equiv h\nu/\sigma_{gsa}\tau$ is the pump saturation intensity. When $I/I_{sat} \ll 1$, the excited state population is given to an excellent degree of approximation by $N_1 \sim N_t(I/I_{sat})$. Hence the factor in Equation (5) describing the contribution of ETU is,

$$\delta \equiv N_1\gamma\tau \cong \beta\frac{I}{I_{sat}} \tag{7}$$

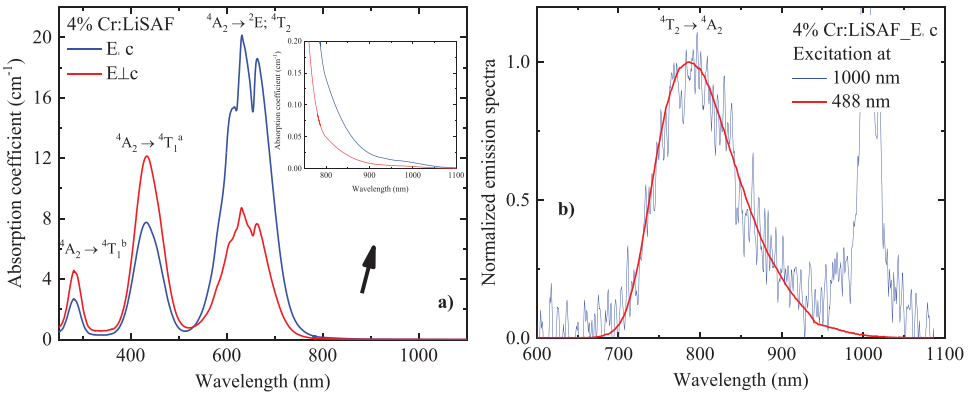

Figure 2. a) Absorption and (b) emission spectra of a 4% Cr^{3+}:LiSAF sample.

where N_t is the total ion concentration and $\beta = N_t \gamma \tau$. Since δ and ξ are both related to excited state processes (ETU and ESA) they are both seen to be proportional to I/I_{sat}.

In this work, thermal lens spectroscopy (TLS)[16] was performed primarily to determine the cooling efficiency of Cr^{3+}:LiSAF crystals. TLS measurements can additionally provide insights into the nonlinear aspects of thermal lens formation in this material which serve to justify the assumptions of our analysis. This point can be made evident by scrutinizing the amplitude of the thermal signal, which is nearly equal to the TLS phase shift parameter, defined as:[17,18]

$$\theta_{th} = \frac{P_{abs}}{\kappa \lambda_p} \varphi \frac{ds}{dT} \tag{8}$$

In this expression $P_{abs} = P_{exc}\, \alpha_t L_{eff}$ is the absorbed power, where P_{exc} is the excitation power, $L_{eff} = (1 - e^{-\alpha_t L})/\alpha_t$ is the effective sample thickness, $\alpha_t = \alpha + \alpha_b$ is total absorption coefficient (due to dopant ions + background) and L is its actual thickness. κ is the thermal conductivity, ds/dT is the temperature coefficient of the optical pathlength change in the sample at the probe laser wavelength, λ_p. The fraction of absorbed energy that is converted into heat in the sample, φ, is defined in Equation (5). It is evident from Equation (8) that the phase shift parameter, and through it the thermal lens amplitude, is proportional to $\varphi = -\eta_c$, where η_c is the cooling efficiency. Consequently, as mentioned previously, TLS can be used as an experimental methodology to determine η_c.[19,20]

To analyze the dependence of the TLS signal on nonlinear dynamics, it is helpful to rewrite Equation (8) as:

$$\theta_{th} = -P_{abs} \Theta_p \eta_c \tag{9}$$

where $\Theta_p \equiv (ds/dT)/\kappa\lambda_p$ is a fixed parameter which depends on the thermo-optical properties of the host crystal. Equation (5) then makes it clear, through the dependence of η_c on δ and ξ, that in general the TLS signal and the cooling efficiency are strongly affected by the nonlinear processes of ETU and ESA. Fortunately, however, in the wavelength range where cooling takes place, absorption is small and the detuning from resonance is large. Consequently, the value of I_{sat} is high and the approximation $I/I_{sat} \ll 1$ is appropriate. The ETU and ESA factors δ and ξ are both small, so that an approximate analysis is justified. Upon inserting Equation (5) into Equation (9) and making a second order expansion in I/I_{sat}, the dependence of the thermal lens signal on ETU and ESA reduces to:

$$\theta_{th} \sim \Theta_p \alpha L_{eff} P_{exc} \left\{ 1 - \eta_{abs}\eta_{ext} \frac{\lambda_{exc}}{\langle \lambda_{em} \rangle} \left[1 - \left(\beta + \frac{\sigma_{esa}}{\sigma_{gsa}} \right) \frac{I}{I_{sat}} \right] \right\} \tag{10}$$

where we note that $I/I_{sat} = P_{exc}/(\pi w_e^2 I_{sat})$. Here, the excitation beam radius is defined as w_e.

2. Results and Discussion

Absorption and emission spectra provide essential information when studying new materials for laser-induced anti-Stokes fluorescent cooling. **Figure 2** presents the spectra for the 4% Cr^{3+}:LiSAF sample analyzed in this work. As shown in Figure 2a, the highest absorption coefficient is observed on transitions from the ground to the first excited states ($^4A_2 \rightarrow {}^4T_2, {}^2E$) for π-polarization of the pump field. The opposite behavior is true for the $^4A_2 \rightarrow {}^4T_1{}^b$ transition. As the energies differ little between the $^4A_2 \rightarrow {}^4T_2, {}^2E$ and the $^4T_2 \rightarrow {}^4T_1{}^a$ transitions, ESA is strong

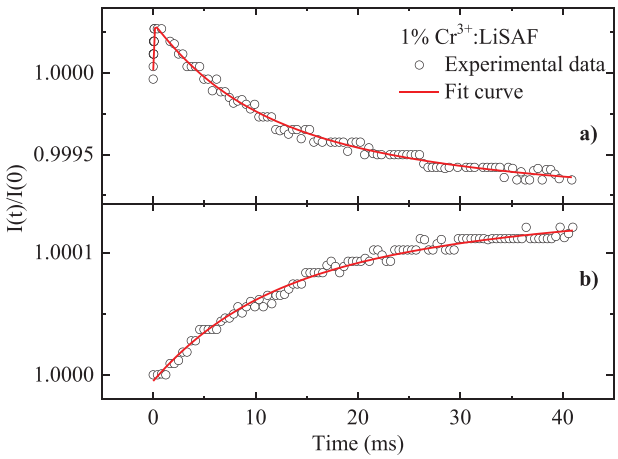

Figure 3. TLS transient signals for an unoriented 1% Cr^{3+}:LiSAF sample measured at a) 751 nm with 522 mW and b) 891 nm using 1265 mW.

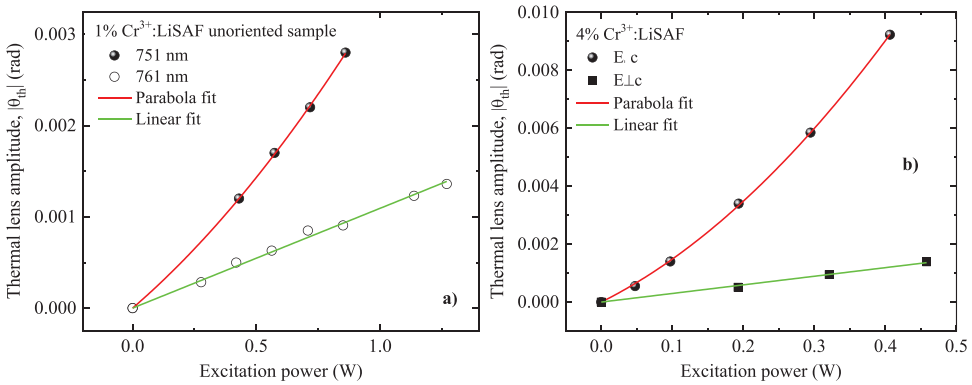

Figure 4. Thermal lens amplitude versus excitation power in a) an unoriented 1% Cr^{3+}:LiSAF sample excited at wavelengths 751 and 761 nm, and b) an oriented 4% Cr^{3+}:LiSAF sample, excited at 751 nm with π- and σ-polarizations.

mainly in σ-polarization.[13] In fact, Rapoport and Shand report no gain for a 7.4% Cr^{3+}:LiSAF sample in σ-polarization, likely due to the presence of ESA.[13] Hence, in this system the choice of π-polarization is not just a matter of obtaining a higher absorbed power, but also of minimizing the undesirable ESA process.

The inset in Figure 2a indicates that the absorption tail of the first resonance extends over 100 nm toward the infrared. Hence, a wide range of detuning can, in principle, excite the sample at long wavelengths, resulting in anti-Stokes fluorescence with an average emission wavelength ≈850 nm.[15] The two emission spectra shown in Figure 2b indicate that anti-Stokes luminescence is indeed observed and that its line shape does not depend on the excitation wavelength. The two recorded spectra for excitation at 488 and 1000 nm are perfectly overlapped, and the anti-Stokes fluorescent spectrum for excitation at ≈1 μm confirms the breadth of the absorption data displayed in the inset of Figure 2a.

Figure 3 shows normalized TLS transient signals in an unoriented 1% Cr^{3+}:LiSAF sample at two different excitation wavelengths, maintaining the same probe wavelength ($\lambda_p = 488\ nm$). Since $\langle\lambda_{em}\rangle = 850\ nm$, heating is expected with $\lambda_{exc} = 751\ nm$, where the transient signal of Figure 3a indicates $\theta_{th} < 0$, which corresponds to a negative (divergent) lens, as a result of $ds/dT < 0$. The opposite behavior is observed at 891 nm, indicative of cooling (Figure 3b) as expected for $\lambda_{exc} > \langle\lambda_{em}\rangle$, if background absorption, ETU and ESA processes are all minimal. It is worth mentioning here that LiSAF is a uniaxial crystal with strong anisotropic thermo-optical properties. Hence, ds/dT can change sign according to the crystal orientation, as shown in previous TLS studies.[21] However, during the scan of the excitation wavelengths, the sample orientation for measurements in Figure 3 was fixed, so the observed signal reversal does indeed indicate that the sample cools at 891 nm. Both transient curves were fitted using a simple expression,[18] which provides the parameters θ_{th} and t_c related to the amplitude and response time, respectively. The thermal diffusivity (D) of the crystal may be obtained from the analysis using $t_c = w_e^2/4D$[16,17] and both transients agreed with $D \sim (8.9 \pm 0.7) \times 10^{-3} cm^2 s$. While the slow transient signals (~ milliseconds) are due to heat diffusion, a fast *population lens* signal is observed in the beginning of the transient shown in Figure 3a. This effect was reported in this material previously and is attributed to the refractive index change caused by differing polarizabilities of the excited and ground states.[18]

In **Figure 4** we investigated the behavior of θ_{th} versus P_{exc} in two different Cr^{3+}:LiSAF crystals. The unoriented 1% Cr^{3+}:LiSAF sample displayed linear behavior with excitation at 761 nm and nonlinear behavior at 751 nm (Figure 4a). We should remark that no nonlinear absorption due to saturation or ESA was observed for all power and wavelength ranges considered in this study. In fact, the linear behavior agrees with Equation (8) if the parameter φ remains constant, indicating the absence of ESA and ETU. On the other hand, significant nonlinear behavior was observed at 751 nm. The data is well fitted by a parabola Equation (10), which considers the effects of ESA and ETU. At 751 nm the absorption coefficient, $\alpha \sim 0.125\ cm^{-1}$, is at least three orders larger than α_b, so $\eta_{abs} \sim 1$ was assumed. A value of $\eta_{ext} \sim 1$ was also assumed since the experiments were performed at a temperature of ~ 16° C where the effect of thermal quenching is expected to be negligible in Cr^{3+}:LiSAF.[15] For $P_{exc} = 0.75\ W$ we then estimated $I/I_{sat} = 4.3 \times 10^{-3}$. The fit results make it possible to deduce the thermo-optic parameter $\Theta_p = (0.47 \pm 0.09)\ W^{-1}$ and the nonlinear factor $(\beta + \sigma_{esa}/\sigma_{gsa}) = 10.4$. Cr^{3+}:LiSAF is known to present a broad ESA band centered at ≈840 nm due to the $^4T_2 \rightarrow {}^4T_1$[a] transition.[13] Although the σ_{esa} value is not known at 751 nm, we estimated $\sigma_{esa}/\sigma_{gsa} \approx 4$, resulting in $\beta \sim 6.4$. Consequently, $\gamma \sim 11 \times 10^{-16} cm^3/s$ was obtained from Equation (7), which is in fair agreement with previously published values.[14] For $\lambda_{exc} = 761\ nm$ the absorption was reduced by half, so the effects of ETU and ESA were weaker, and the observed behavior was nearly linear.

In addition to the unoriented 1% Cr^{3+} crystal, an oriented 4% Cr^{3+}:LiSAF sample was available that permitted π- or σ-polarized excitation of TLS transients (with electric field E parallel or perpendicular to the optic axis c, respectively). Figure 4b shows thermal lens amplitudes observed at 751 nm for both polarizations. A linear behavior is observed for $E \perp c$ and a parabolic one for $E \| c$. The difference is attributed to the stronger absorption obtained with π-polarization (Figure 2). At $\lambda_{exc} = 751\ nm$, the absorption cross-section for π-polarization is 2.8 times greater than for σ-polarization, so nonlinear behavior is only observed for $E \| c$. The fit with Equation (10) results in $\Theta_p = 0.55 \pm 0.11\ W^{-1}$, $(\beta + \sigma_{esa}/\sigma_{gsa}) = 145$ and $\gamma \sim 60 \times 10^{-16} cm^3/s$. As previously observed in LiSAF,[10,14] the γ parameter increases approximately linearly with Cr concentration so β

Table 1. Some optical parameters for the Cr^{3+}:LiSAF crystal with 1 and 4 at.% of Cr^{3+}. * Calculated using data from reference 10.

Parameters	Value	Units
Upconversion parameter, γ	11 (1%) and 60 (4%)	10^{-16} cm^3/s
Lifetime,[15] τ	67	μs
Total ion concentration,[10] N_t	0.875 (1%) and 3.53 (4%)	10^{20} cm^{-3}
External quantum efficiency,[18] η_{ext}	1	
Average emission wavelength,[15] $\langle\lambda_{em}\rangle$	850	*nm*
Pump saturation intensity*, $I_{sat}(750-1090\ nm)$	1.6 – 653	*MW*/cm^2
ESA cross-section,[13] $\sigma_{esa}(750-1090\ nm)$	(2.0 – 2.2)	10^{-20} cm^2

increases quadratically. **Table 1** summarizes the results obtained in this work and those from literature needed to perform the calculations.

Figure 5 displays the cooling efficiency (η_c) versus excitation wavelength (λ_{exc}) determined by TLS for both samples evaluated in this work.[22] Each data point was obtained from a linear plot of θ_{th} versus excitation power. The fit with Equation (5) was performed by fixing the parameters $\eta_{ext} = 1$ and $\langle\lambda_{em}\rangle = 850\ nm$. These two assumed values are supported by well-established experimental data.[10–15] For the 1% Cr^{3+}:LiSAF sample (Figure 5a), a maximum cooling efficiency of ≈10% was observed at ≈1 μm. Interesting insight into the cooling mechanism can be obtained by analyzing the crossing wavelength (λ_{cr}), which is the excitation wavelength in which $\eta_c = 0$. According to Equation (5) this wavelength is given by $\lambda_{cr} \sim \langle\lambda_{em}\rangle[\eta_{ext}\eta_{abs}(1-\delta-\xi)]^{-1}$. From the data of Figure 5a, an experimental value of $\lambda_{cr} \sim 861\ nm = 1.013\langle\lambda_{em}\rangle$ is obtained, indicating a 1.3% increase relative to $\langle\lambda_{em}\rangle$, attributed to various loss mechanisms. At 861 nm we estimated that I/I_{sat} is not higher than 2.5×10^{-4}, which implies that the factor $(\delta+\xi)$ is less than 2.5×10^{-3}, and therefore nearly negligible. By assuming $\eta_{ext} = 1$ and $(\delta+\xi) = 0$, an efficiency factor of $\eta_{abs} \sim 0.987$ may be estimated, suggesting that the main loss is due to background absorption with a coefficient of $\alpha_b = (9\pm7)\times10^{-5}$cm^{-1}. The green curve in Figure 5a is based on this value.

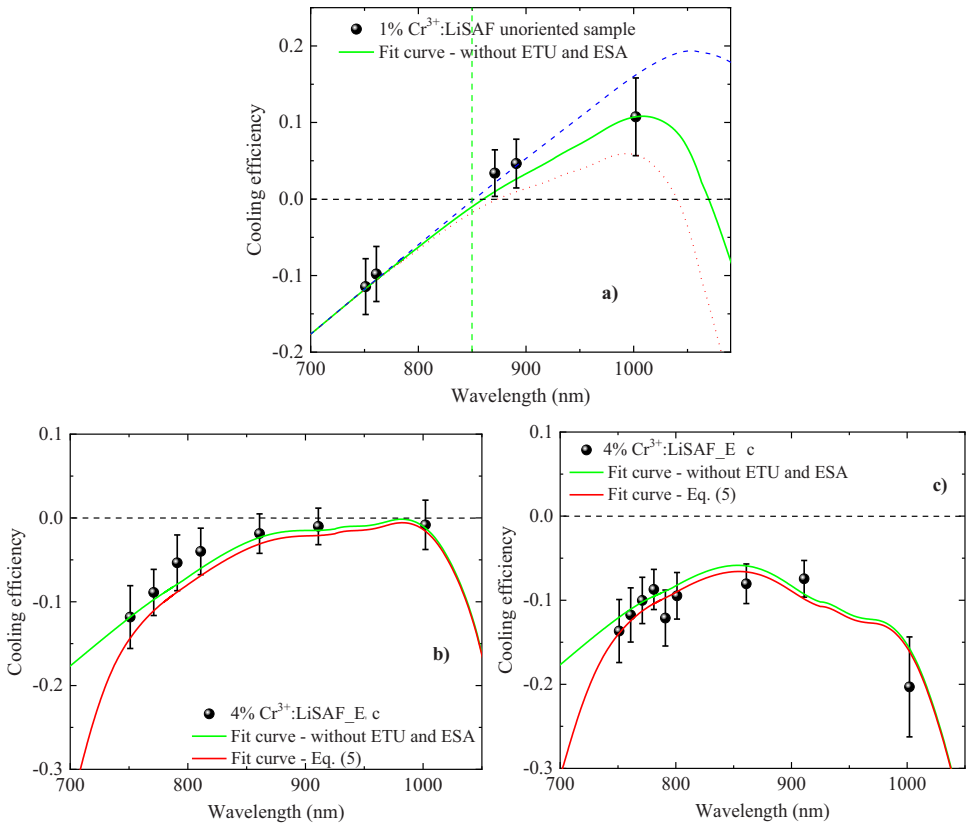

Figure 5. Cooling efficiency for a a) 1% Cr^{3+}:LiSAF unoriented sample and 4% Cr^{3+}:LiSAF in b) π-polarization, and c) σ-polarization. The green straight curves omit excited state dynamics while the red straight curves consider them together with b) $\omega_e = 100$ μm, c) $\omega_e = 70$ μm, and $P_{exc} = 0.1\ W$. The thermo-optic parameters were b) $\Theta_p = -0.55\ W^{-1}$, c) $\Theta_p = -0.32\ W^{-1}$, and the Auger and ESA parameters were $\delta \approx 10^{-2} - 10^{-5}$ and $\xi \approx 10^{-3}$ respectively.

The dotted red and dashed blue lines are simulations based on background absorption at the limits of the error bars in the determination of α_b.

Figure 5b,c shows the cooling efficiency results for the 4% Cr^{3+}:LiSAF sample in both polarizations. As mentioned before and shown in Figure 4, the ETU effect is much stronger in the 4% crystal than in the 1% one. Therefore, to ascertain whether nonlinearities affected the cooling efficiency itself, two fits were made for each polarization. The fits were made with Equation (5) first using the parameters of Table 1 to include ETU and ESA in the red curves and then with $\xi = \delta = 0$ to exclude these nonlinearities in the green curves. For the red curves the parameters ξ and δ were calculated at each wavelength based on the wavelength dependence of σ_{gsa} and σ_{esa},[13] while the ETU parameter was fixed with a value of $\gamma = 6 \times 10^{-15}$ cm^3/s. The Θ_p values used in the fits agreed rather well with published values,[14,15,18] taking into account the uncertainties of prior measurements (see the caption of Figure 5). As a result, α_b was the only adjustable parameter to be determined by the fits, yielding a value of $\alpha_b = (1.8 \pm 0.2) \times 10^{-3} cm^{-1}$ for π-polarization. For σ-polarization, the corresponding value was $\alpha_b = (1.3 \pm 0.2) \times 10^{-3} cm^{-1}$. Although the derived α_b values are ≈30% larger for π- than σ-polarization, we note that the η_{abs} was a factor of ≈3 higher for π due to its larger cross-section σ_{gsa}. Consequently, the best cooling efficiency was obtained exciting with π-polarization in this sample (Figure 5b,c, respectively). A strong reduction of the heat generated in the sample was observed for π-polarized light, and the sample reached the cooling threshold at a wavelength of 1 μm. On the other hand, the results for the σ-orientation are relatively far below the cooling threshold at all wavelengths. It is interesting to notice that laser oscillation in Cr^{3+}:LiSAF is also better for π-polarization due to a higher ratio of stimulated emission to ESA cross-sections, as mentioned by Rapoport and Shand.[13]

For the 4% Cr^{3+}:LiSAF sample in the 800–1000 nm spectral range, the fits with and without ESA and ETU effects yielded almost identical predictions. It should be noted that the absorption cross-section decreases two orders of magnitude from 750 to 1000 nm. Hence although nonlinear contributions to thermal lensing were observable at 751 nm (Figure 4b) the strong decrease of the saturation ratio I/I_{sat} at longer wavelengths undoubtedly diminishes the deleterious effects of ESA and ETU in this range. Finally, we note that the parasitic background absorption coefficients (α_b) determined from fits that included or omitted excited state dynamics for a given polarization were the same within experimental error. However, the best fit value of α_b for π-polarization was slightly higher than for σ-polarization. This may be an effect of crystal anisotropy on the impurity absorption, as observed in high-purity undoped YLF crystals where a higher parasitic background absorption was reported for π-polarization compared to σ-polarization.[23] Additionally, the much higher background absorption presented by the 4% crystal compared to the 1% one indicates that the CrF_3 doping may have the source of parasitic impurity that impact on α_b. Hence, the growth of ultra-pure higher Cr^{3+}-doped LiSAF samples should be worthwhile to realize even better cooling performance of this promising material for optical refrigeration.

Table 2. Maximum cooling efficiencies (η_c) experimentally achieved in rare-earth doped crystals with average emission $\langle\lambda_{em}\rangle$ and excitation λ_{exc} wavelengths. Our results in 1% Cr^{3+}:LiSAF are also presented for comparison.

Material	λ_{exc}[nm]	$\frac{\lambda_{exc}-\langle\lambda_{em}\rangle}{\langle\lambda_{em}\rangle}$ [%]	η_c [%]	Refs.
Yb^{3+}:$LiYF_4$	1060	6.0	5.0	[2,20]
Er^{3+}:KPb_2Cl_5	870	2.1	0.68	[4]
Tm^{3+}:BaY_2F_8	1930	7.6	3.5	[3]
Ho^{3+}:$LiYF_4$	2150	6.7	2.5	[5]
Cr^{3+}:$LiSrAlF_6$	1000	18	10	This work

Finally, to demonstrate the importance of the findings of this work to the field of laser cooling of solids, **Table 2** presents a list of cooling crystalline materials doped with different rare-earth ions along with the 1% Cr^{3+}:LiSAF sample studied in this work. It can be seen that Cr^{3+}:LiSAF yields twice the cooling efficiency of the best solid-state cooling material reported so far (Yb^{3+}:YLF). In its third column, the table still presents an ideal cooling, when ETU, ESA and α_b are negligible and $\eta_{ext} = 1$.

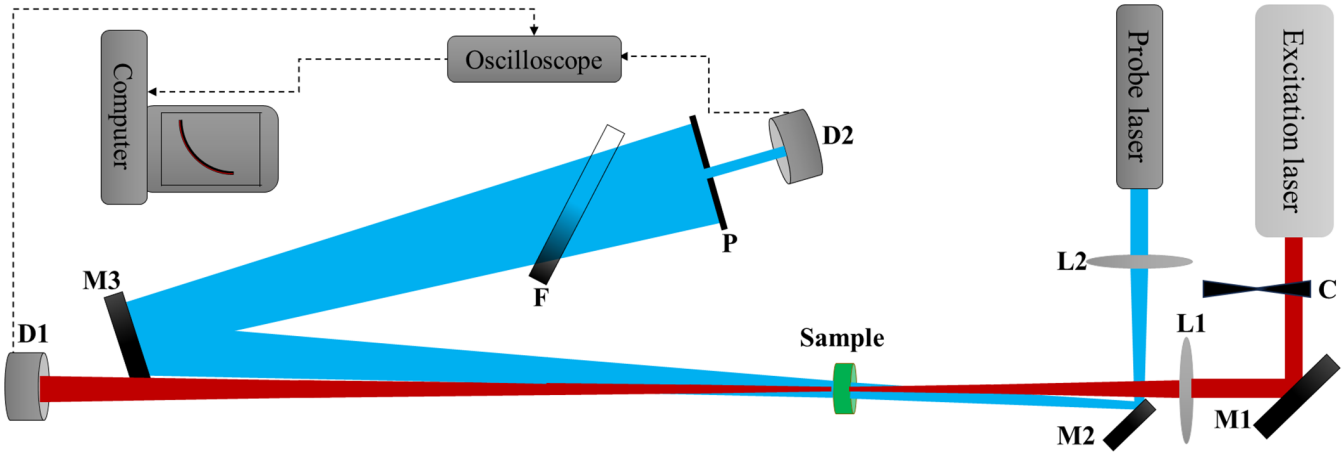

Figure 6. Setup used in the TLS experiments. The labels indicate M-mirror, L-lens, C-chopper, D-photodetector, F-spectral filter, and P-pinhole.

3. Conclusion

In this work, an ED-allowed optical transition was used to evaluate laser cooling efficiencies in 1% Cr^{3+}:LiSAF and 4% Cr^{3+}:LiSAF crystals. TLS measurements revealed that the 1% Cr^{3+}:LiSAF sample cooled at wavelengths longer than the average emission wavelength (850 nm), reaching a maximum cooling efficiency of ≈10%. In the 4% Cr^{3+}:LiSAF sample, the cooling threshold was reached for π-polarized excitation at $\lambda_{exc} \approx 1000\ nm$. The absence of net cooling in 4% Cr^{3+}:LiSAF was attributed to the relatively high parasitic background absorption ($\sim 1.8 \times 10^{-3}\ cm^{-1}$) of the available sample. Notably, both samples presented maximum cooling efficiency at $\lambda_{exc} \sim 1000\ nm$, corresponding to $(\lambda_{exc} - \langle\lambda_{em}\rangle)/\langle\lambda_{em}\rangle \sim 18\%$ which compares very favorably with values of ≈6% in Yb^{3+}-doped materials. This suggest that Cr^{3+}:LiSAF has the potential to achieve cooling efficiency at least three times higher than Yb^{3+}-doped materials, provide that parasitic absorption can be reduced to $\alpha_b \sim 10^{-5} cm^{-1}$ for 1% Cr^{3+} concentration, or $10^{-4}cm^{-1}$ for 4% Cr^{3+} concentration. It was also ascertained that at the intensity levels used in the present experiments, ETU and ESA did not play a significant role in limiting the cooling efficiency.

4. Experimental Section

The optical spectroscopic analyses were carried out using commercial Shimadzu instrumentation. Absorption spectra were recorded with a spectrophotometer (model UV-3600), and luminescence spectroscopy was performed using a model RF-6000 spectrometer. Both samples were grown by AC Materials, Inc., and they had the following dimensions: (12 × 11 × 3.5) mm for the 1% Cr:LiSAF, in which the thickness (*L*) was 3.5 mm. For the 4% Cr:LiSAF, it was (2.8 × 2.8 × 10) mm. The thickness to pump E||c and E⊥c was 2.8 mm.

A multiwavelength mode-mismatched dual-beam configuration was used in the TLS measurements. A gradient temperature was generated in the sample using a single-mode Ti:sapphire laser operating in the 750–1000 nm range. An optically pumped semiconductor laser operating at 488 nm in a single mode was used to probe the thermal lens-like element. **Figure 6** shows the TLS setup used in our experiments. The sample was positioned in the waist of the mechanically chopped excitation beam, and the transmitted beam was detected with a photodiode to provide a triggering signal. An optical filter was used to avoid scattered radiation from the pump beam at the detector (D2). The intensity at the center of the probe beam was monitored as a function of time and the transient signals were analyzed to provide the thermal lens amplitude from which the experimental cooling efficiency was calculated. Additional details on this setup and TLS in Cr^{3+}:LiSAF crystals can be found elsewhere.[14–18]

Acknowledgements

The authors gratefully acknowledge support from the Fundação de Apoio ao Desenvolvimento do Ensino, Ciência e Tecnologia do Estado de Mato Grosso do Sul (71/032.546/2022) and from the Conselho Nacional de Desenvolvimento Científico e Tecnológico (308242/2022-0). The authors are also grateful for support from the University of Michigan, where the measurements were made.

The Article Processing Charge for the publication of this research was funded by the Coordenação de Aperfeiçoamento de Pessoal de Nível Superior - Brasil (CAPES) (ROR identifier: 00x0ma614).

Conflict of Interest

The authors declare no conflict of interest.

Data Availability Statement

The data that support the findings of this study are available from the corresponding author upon reasonable request.

Keywords

anti-stokes fluorescence, Cr3+:LiSAF, electric dipole allowed transitions, optical refrigeration, thermal lens spectroscopy

Received: November 22, 2024
Revised: May 12, 2025
Published online: May 27, 2025

[1] R. I. Epstein, M. I. Buchwald, B. C. Edwards, T. R. Gosnell, C. E. Mungan, *Nature* **1995**, *377*, 500.
[2] S. D. Melgaard, A. R. Albrecht, M. P. Hehlen, M. Sheik-Bahae, *Sci. Rep.* **2016**, *6*, 20380.
[3] W. Patterson, S. Bigotta, M. Sheik-Bahae, D. Parisi, M. Tonelli, R. Epstein, *Opt. Exp.* **2008**, *16*, 1704.
[4] J. Fernandez, A. J. Garcia-Adeva, R. Balda, *Phys. Rev. Lett.* **2006**, *97*, 033001.
[5] S. Rostami, A. R. Albrecht, A. Volpi, M. Sheik-Bahae, *Photonics Res.* **2019**, *7*, 445.
[6] B. Topper, S. Kuhn, A. Neumann, A. R. Albrecht, A. S. Flores, D. Hässner, S. Hein, C. Hupel, J. Nold, N. Haarlammert, T. Schreiber, M. Sheik-Bahae, A. Mafi, *Opt. Exp.* **2024**, *32*, 3660.
[7] M. P. Hehlen, *J. Lum.* **2022**, *252*, 119270.
[8] S. P. Feofilov, A. B. Kulinkin, *Opt. Mater.* **2018**, *75*, 554.
[9] S. P. Feofilov, A. B. Kulinkin, *Opt. Mater.* **2019**, *94*, 231.
[10] U. Demirbas, *Prog. Quant. Elect.* **2019**, *68*, 100227.
[11] S. A. Payne, L. L. Chase, L. K. Smith, W. L. Kway, H. W. Newkirk, *J. Appl. Phys.* **1989**, *66*, 1051.
[12] L. Cheng, L. B. Andre, D. Rytz, S. C. Rand, *Opt. Exp.* **2023**, *31*, 11994.
[13] W. R. Rapoport, M. L. Shand, *Sol. St. Commun.* **1992**, *84*, 29.
[14] V. Pilla, T. Catunda, H. P. Jenssen, A. Cassanho, *Opt. Lett.* **2003**, *28*, 239.
[15] V. Pilla, T. Catunda, S. Marcio Lima, A. Neto Medina, M. Luciano Baesso, H. P. Jenssen, A. Cassanho, *J. Opt. Soc. Am. B* **2004**, *21*, 1784.
[16] J. Shen, R. D. Lowe, R. D. Snook, *Chem. Phys.* **1992**, *146*, 385.
[17] J. R. Silva, L. C. Malacarne, M. L. Baesso, S. M. Lima, L. H. C. Andrade, C. Jacinto, M. P. Hehlen, N. G. C. Astrath, *Opt. Lett.* **2013**, *38*, 422.
[18] J. R. Silva, T. Catunda, S. C. Rand, *Opt. Lett.* **2023**, *48*, 6541.
[19] J. R. Silva, L. H. C. Andrade, S. M. Lima, M. P. Hehlen, Y. Guyot, A. N. Medina, L. C. Malacarne, M. L. Baesso, N. G. C. Astrath, *App. Phys. Lett.* **2013**, *102*, 141910.
[20] J. R. Silva, L. H. C. Andrade, S. M. Lima, Y. Guyot, N. Giannini, *Opt. Mat.* **2019**, *95*, 109195.
[21] A. Steimacher, O. A. Sakai, A. C. Bento, M. L. Baesso, A. N. Medina, S. M. Lima, T. Catunda, *Opt. Lett.* **2008**, *33*, 1720.
[22] S. M. Lima, A. A. Andrade, R. Lebullenger, A. C. Hernandes, T. Catunda, M. L. Baesso, *App. Phys. Lett.* **2001**, *78*, 3220.
[23] M. P. Hehlen, J. Meng, A. R. Albrecht, E. R. Lee, A. Gragossian, S. P. Love, C. E. Hamilton, R. I. Epstein, M. Sheik-Bahae, *Light: Sci. Appl.* **2018**, *7*, 15.